A Review of Lidar for Self-Driving Cars

Author: Thomas Hartigan, Supervisor: David Buscher

ABSTRACT

Autonomous driving promises to save millions of lives per year by reducing the frequency of driver-error road accidents. It is widely accepted by automotive manufacturers, apart from Tesla, that any autonomous driving system will require the incorporation of light detection and ranging (LIDAR or lidar) technology to detect the environment surrounding the vehicle with sufficient accuracy to support reliable hazard detection. This review discusses the specifications, such as minimum detection range, field of view, angular resolution, sampling rate, eye safety and resilience to adverse environmental conditions that automotive lidar must reach to support fully autonomous driving. Technological advances that have supported the development of these systems to their current level are also discussed, with explorations of pulsed and coherent lidars, scanning methods, illumination technologies and receiver technologies. Furthermore, details of current and upcoming commercial automotive lidar systems are presented, along with a discussion of future technological and academic advances, including a brief discussion of the machine learning methods being used to advance lidar data analysis.

1. Introduction

Lidar (light detection and ranging) for self-driving applications has progressed rapidly in the past 20 years, evolving from large, mechanically driven detectors [1] to solid-state technologies capable of millions of detections per second at over 200m range. This review aims to offer a more holistic view of automotive lidar hardware than that offered in previous works [2–7].

An overview of technological advancements follows in §2, before the specific requirements and limitations of lidar for autonomous driving are discussed in §3. Finally §4 discusses the state of modern and future automotive lidar technology, and conclusions are presented.

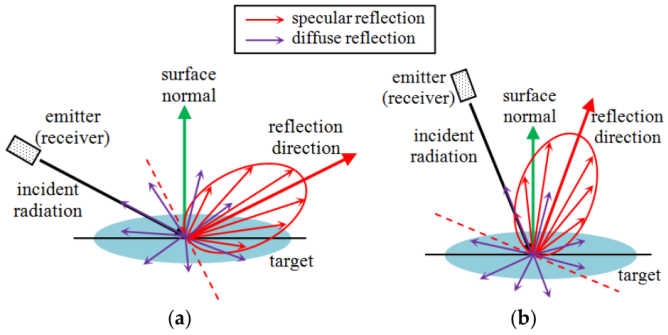

Fig. 1. Contributions of specular and diffuse reflections to backscattered radiation at incident angles (a) > 45° and (b) < 45° [8]

2. Automotive Lidar Technology

2.1. Operating Principles

Lidar systems build up images of their environment by emitting laser pulses at near-infrared frequencies [2–5]. Upon collision with matter, these pulses scatter, directing some of the energy back towards the emitter. This returned energy is then detected as photons by the lidar system.

2.1.1. Pulsed Lidar

The reflected power, P_r, detected by a lidar system from a laser emitter can be modelled as

$$P_r = P_0 \frac{\eta A_r}{r^2} \beta T_r \,, \tag{1}$$

where P_0 is the peak output power of a transmitted pulse, η is the receiving optics spectral transmission, A_r is the area of the primary receiver optics, r is the range from the (coincident) laser source and detector to the target, β is the reflectivity of the target, and T_r denotes the transmission loss through the atmosphere [9, 10]. These transmission losses are often due to rain, fog or dust particles suspended in air. For a lidar system to be successful in detecting a target, it must be capable of detecting returns as small as P_r (see §2.4).

The specular and diffuse components of reflections depend on the incident angle of the laser on the target surface (see Figure 1). However, in the idealised case where the laser is incident on a Lambertian surface (an ideal diffusion surface) with reflectance ($0 < \Gamma < 1$) the reflectivity of the target's surface [8],

$$\beta = \frac{\Gamma}{\pi} \,. \tag{2}$$

Detection can therefore be improved most readily by increasing η, A_r, or P_0, subject to eye safety requirements (§3.2).

Measuring the time between emission and detection of a reflected pulse, Δt, allows for calculation of the distance to the target

$$r = \frac{1}{2n} c \Delta t \,, \tag{3}$$

where n is the refractive index of the propagation medium (≈ 1 for air) [3]. Where δ represents uncertainty, the associated ranging resolution is therefore

$$\delta r = \frac{1}{2n} c \delta(\Delta t) \,. \tag{4}$$

2.1.2. Coherent Lidar

Continuous lidar methods include frequency modulated continuous wave (FMCW), amplitude modulated continuous wave (AMCW), and random modulation continuous wave (RMCW) emissions [11]. Compared with pulsed lidars, these transmit with lower power, but allow the received energy to accumulate for longer whilst adhering to eye safety requirements, effectively increasing P_0 in (1), and therefore improving detection performance.

The most promising of these for future developments, FMCW, can work by modulating the transmission frequency following a triangular chirp (see Figure 2) and measuring the instantaneous difference between the frequency of the emitted and detected signals (the intermediate frequency, IF). The IF, f_{if}, can be found using a homodyne configuration of the transmitted and received waves. Once it is known, the range to the target is given by

$$r = \frac{f_{\text{if}} T c}{4B}, \tag{5}$$

where B is the modulation bandwidth and T is the period of the triangular chirp [12]. If the target is moving, then the received signal will also be Doppler shifted by frequency, f_{d}. Hence, during the up-ramp and down-ramp, the detected IFs are $f_{\text{if}}^{+} = f_{\text{if}} + f_{\text{d}}$ and $f_{\text{if}}^{-} = f_{\text{if}} - f_{\text{d}}$ respectively. In the presence of a Doppler shift, f_{if} in (5) can be found using

$$f_{\text{if}} = \frac{f_{\text{if}}^{+} + f_{\text{if}}^{-}}{2}. \tag{6}$$

The Doppler shift itself can also be found using

$$f_{\text{d}} = \frac{f_{\text{if}}^{+} - f_{\text{if}}^{-}}{2}, \tag{7}$$

and therefore, the velocity of the target can be found as

$$v = \frac{f_d \lambda}{2 \cos\theta}, \tag{8}$$

where λ is the transmitter laser wavelength and θ is the angle between the target velocity vector and the lidar line of sight [4, 12, 14, 15]. As FMCW lidar is capable of simultaneously detecting range and velocity, it provides a fourth dimension of data, which can assist object identification and future path prediction (see §4), giving increased system reliability and self-driving safety [13, 17].

2.2. Scanning Methods

Diffraction gives the angular divergence of a beam emerging from an aperture (such as a lidar lens or mirror) as

$$\alpha = 1.22 \frac{\lambda}{D}, \tag{9}$$

where D is the aperture diameter [4]. Hence, using $\lambda = 850$nm with $D = 1$cm at a range of 200m, it could be possible to discern objects 3cm apart. By directing the laser precisely, it is therefore possible to image the surrounding environment in detail, even at large distances, so long as a detectable amount of energy is returned. The most widely used beam-steering methods are discussed below. However, new technologies such as chip-scale acousto-optic beam steering [16] are also emerging.

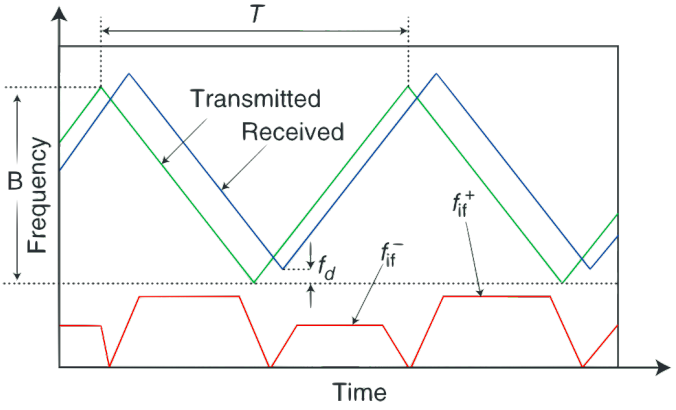

Fig. 2. Transmitted, received, and intermediate frequencies for triangularly chirped FMCW transmissions [12].

2.2.1. Mechanical Scanning

Mechanical scanning is the most rudimentary beam-steering method, physically rotating the laser sources and detectors, or a mirror. This allows one lidar detector to cover a 360° field of view (FoV), although using many detectors reduces the required motion. This method has seen commercial success, such as with the Ouster VLS-128 detector, with an operational range of 300m at target reflectivity $\beta = 0.1$ [18]. However, these systems typically have high production costs and can be particularly fragile [3], so most companies now use solid-state scanning methods.

2.2.2. Microelectromechanical Scanning (MEMS)

MEMS beam-steering utilises either electrostatic or magnetic actuation mirrors, where a Lorentz force balances a torque acting on the mirror, giving rotational control [19, 20]. These mirrors may be rotated at their resonant frequency (resonant control), giving a wider FoV but irregular sampling, or linearly, giving fine directional control [21].

The cost of MEMS technology is relatively low due to the maturity of near-solid-state technology in the integrated circuit industry [3]. However, the MEMS lidar mirrors introduce further beam divergence [22] and there are concerns about creep and mechanical fracture in micromirror devices [23].

2.2.3. Flash Lidar

Flash lidars emit diffuse pulses of radiation and then detect reflections using spatially separated detectors [3]. Flash lidar systems are truly solid-state, removing the complexity of moving parts. However, due to eye safety limitations (§3.2), the pulse must have limited power. Reflected power density can be improved using a series of 2D (blade) flashes, but detection ranges are still generally under 100m. These systems are therefore most useful for short-range detection tasks, such as lane-changing assistance or pedestrian movement prediction. Recent developments using a series of segmented flashes have achieved ranges over 100m [24]. Furthermore, new processing methods can utilise secondary reflections from an initial flash to image behind obstructions [25].

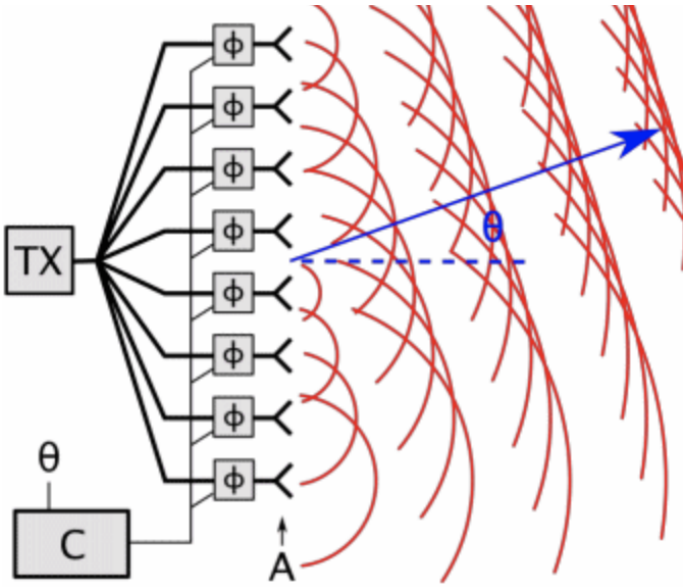

Fig. 3. An optical phased array changing the direction of wavefront propagation [26].

2.2.4. Optical Phased Arrays

Optical phased arrays (OPAs) are truly solid-state and work by introducing an additional phase to a coherent wave emitted by multiple antennae, as depicted in Figure 3. This is done using optical phase modulators to change the speed of light through the lens [3]. Lumotive has previously used liquid crystals to achieve the same effect [4]. OPAs allow for low-cost mass-production using existing chip manufacturing techniques, but realisation of the technology is difficult due to larger beam divergence and high rates of energy loss in OPA components [5].

2.3. Illumination Technologies

Lidar technology for self-driving applications has mostly developed around the 905, 940, and 1550nm wavelengths, due to lower solar irradiance - reducing environmental noise (Figure 4), and lower atmospheric water absorption (Figure 5). To account for the presence of water in the atmosphere, T_r in (1) can be approximated as

$$T_r = \exp(-2\gamma r) \tag{10}$$

where γ is the atmospheric extinction coefficient. The two most common technologies for producing these wavelengths in automotive lidar applications are discussed below.

2.3.1. Vertical Cavity Surface Emitting Lasers (VCSELs)

VCSELs are laser diode chips which exploit Bragg reflections to radiate circular milliwatt beams with high wavelength stability perpendicular to the surface of the wafer on which they are integrated (Figure 6.a) [29]. They can achieve wavelength spectrum full-width half maximum (FWHM) 0.61nm [29] and FWHM beam divergence around 12°. Other silicon components, such as collimation lenses can, however, be integrated on-chip during manufacture to reduce divergence [30]. On-chip manufacturing also significantly reduces cost. Furthermore, VCSELs can be stacked in a 2D array on-chip to increase power output. One implementation [31] reports 100W power output with FWHM divergence 17° and spectral FWHM of 0.8nm.

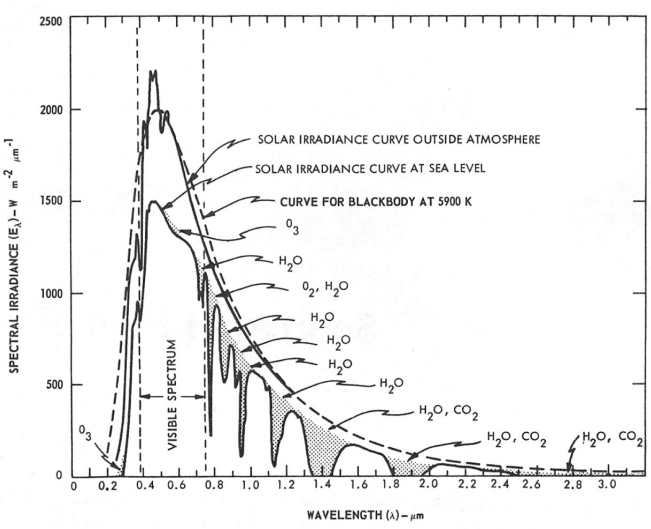

Fig. 4. Spectral solar irradiance outside the atmosphere and at sea level [27, 28].

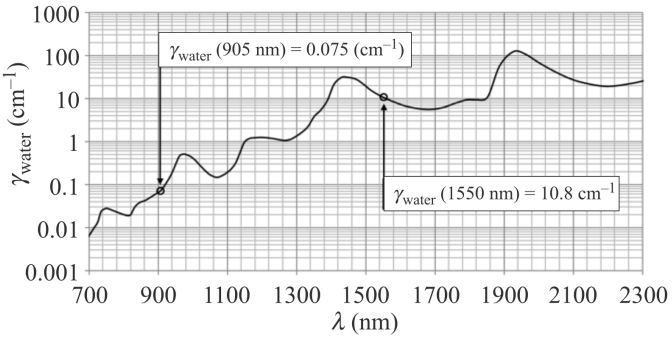

Fig. 5. Water extinction coefficient spectrum for near-infrared frequencies [10]

VCSEL wavelength spectra are resistant to temperature change, shifting only around 0.06nm/K compared to 0.25nm/K for edge-emitting lasers [29]. This makes them particularly well-suited to automotive applications, which require functionality over a 125°C range.

Within this context, VCSELs are mostly used for flash lidars (§2.2.3), utilising their large angular divergence and very low spectral FWHM - enabling rejection of the majority of ambient light using narrow spectral filters [32]. Pulsed VCSELs can also produce high peak output powers, so are expected to be implemented in future scanning lidar systems [36].

2.3.2. Edge-Emitting Lasers (EELs)

EELs are also diode chips, but unlike VCSELs, light oscillates and radiates parallel to the wafer, emitting through coated, cleaved facets, resulting in a highly-divergent, elliptical beam (Figure 6.b) [33].

Historically, EELS have been widely used for automotive lidar, due to their maturity in telecommunications markets and their ability to generate high output powers, particularly when stacked. However, this stacking is expensive and EELs are vulnerable to “catastrophic optical damage” - where high

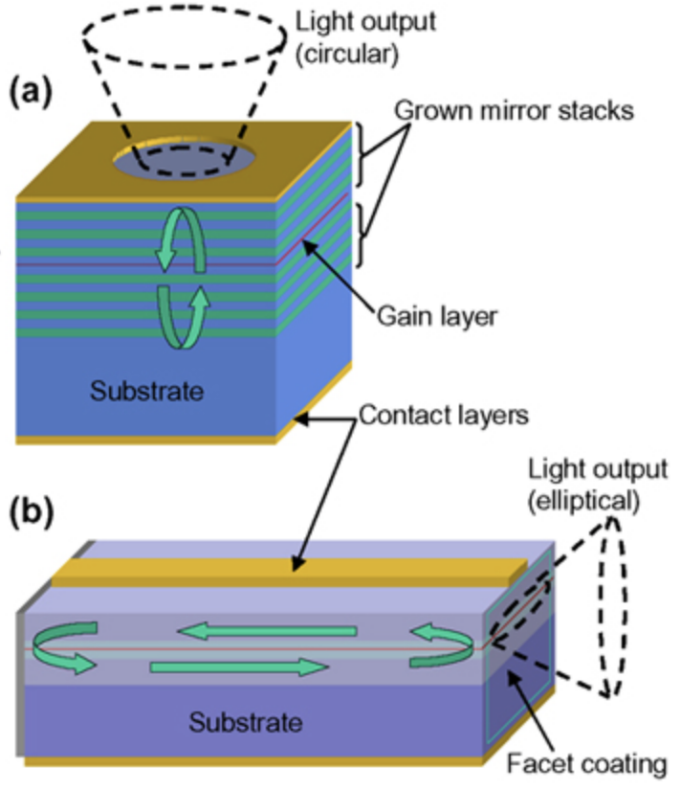

Fig. 6. Schematic representations of (a) VCSELs and (b) EELs [33].

laser mirror temperatures, around 450°C, drive degradation of the emission facets [34]. Furthermore, compared with VCLES, EELs have wider spectral FWHMs of around 3-5nm and much greater emission spectrum shifts with temperature change [29]. This temperature shift can, however, be compensated for [35].

As both EELs and VCSELs can overcome most of their challenges for automotive lidar applications, both can be used for short and long-range detection, with choice of illuminator usually determined by specific system requirements, implementation difficulty and cost [36].

2.4. Receiver Technologies

If an individual detector is capable of detecting n or more photons, then it can be shown from (1) [37] that the required transmitter energy for a pulse to be detected is

$$E_T = \frac{4.4nhc}{\lambda}\frac{N_{\text{det}}}{\beta}\left(\frac{r}{D}\right)^2\frac{e^{2\gamma r}}{\eta}, \tag{11}$$

where N_{det} is the number of detectors used (such as when stacked in a grid), D is the collecting aperture diameter, and all other parameters are as defined previously.

Automotive photodiodes utilise the photoelectric effect to generate an electron-hole pair when a photon collides with an intrinsic semiconductor region. Both the electron and hole are then accelerated by an applied electric field. When these carriers acquire sufficient kinetic energy and collide with atoms in the semiconductor crystal, multiple secondary electrons can be released by impact ionisation. This produces an avalanche reaction, releasing more electrons with each collision, generating a detectable current [6, 37]. Common implementations of this photoelectric avalanche (PEA) method are now discussed.

2.4.1. Avalanche Photodiodes (APDs)

APDs usually use high reverse bias voltage, V_{rev}, below the breakdown voltage of the semiconductor, V_{break}, to accelerate the induced electrons and holes. This results in gains between 50 and 1000 for silicon detectors - capable of detecting signals between 450 and 1000nm and gains between 10 and 40 for indium gallium arsenide (InGaAs) detectors - capable of detection up to around 1700nm [38]. APDs output currents are proportional to the number of incident photons [6] with a sufficiently high bandwidth (GHz, [38]) to produce photocurrent waveforms [37]. However, these systems are unable to reliably detect single photons, due to uncertainty in whether an impact ionisation event triggers an avalanche for $V_{\text{rev}} < V_{\text{break}}$ [6].

2.4.2. Single Photon Avalanche Diodes (SPADS)

SPADs also exploit PEA but operate with $V_{\text{rev}} \gtrsim V_{\text{break}}$ [6], allowing a single electron-hole production event to trigger avalanche detection with around 50% success [38]. This avalanche current increases much more rapidly than that seen in APDs, rising until reaching a steady level (gain $> 10^4$ [6]). At this point, detection is reported and the SPAD resets to its initial state by quenching - generally by setting $V_{\text{rev}} < V_{\text{break}}$ for a short time. This process results in SPAD detectors being inactive for times of the order 100ns, resulting in only HMz bandwidth [38]. Future developments in active quenching may reduce this inoperable time.

SPADs are only sensitive to single events, so may be falsely activated by thermally-generated carriers and afterpulsing - where some carriers from the avalanche get released from deep energy levels in the junction depletion layer after quenching has occurred [39]. This high sensitivity also means that SPAD detectors can be saturated by large reflections, such as those from road signs, rendering them inoperable for short periods [6].

2.4.3. Silicon Photomultipliers (SiPMs)

SiPMs (also known as multipixel photon counters) are arrays of SPADs which linearly combine the output from each SPAD into a joint analogue signal, allowing the number of incident photons, and hence the incident photocurrent to be estimated. This results in very high gain around 10^6 [6], although the linearity of incident photocurrent and signal current does decay with intense illumination due to the increased chance a SPAD has already triggered and has not yet been quenched.

SiPMs suffer from both afterpulsing and optical crosstalk, where the avalanche process in one SPAD can trigger discharges in adjacent SPADs, but are otherwise very well suited to low-light applications, including long-range lidar measurements.

3. Requirements and Limitations of Lidar for Automotive Applications

To provide sufficient data for self-driving applications, automotive lidar systems must detect features of concern from sufficient distance to allow the vehicle to navigate safely.

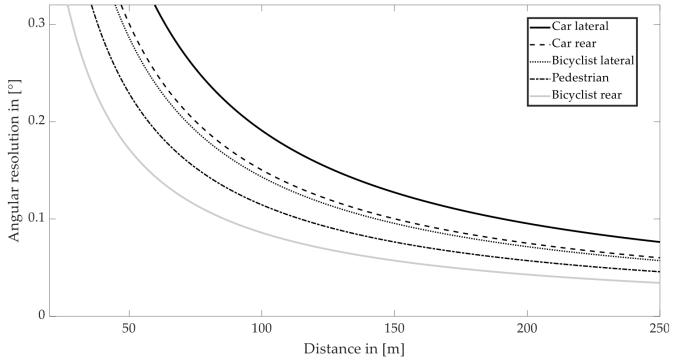

Fig. 7. Angular resolution required to identify objects with 50% confidence for 0-250m ranges [41].

3.1. Long-Range Detection

Long-range applications, such as forward-looking lidar whilst travelling at speeds around 140km/h, require a detection range ≥ 200m [7, 40, 41]. More generally, if an object is moving with relative velocity v_{rel} in front of the subject vehicle, moving with velocity v_1, and the subject vehicle can decelerate at rate a_1, then the required warning distance before collision is

$$D_{\text{warn}} = \left(T + \frac{v_{\text{rel}}}{a_1}\right) v_1 - \frac{v_{\text{rel}}^2}{2a_1}\,, \tag{12}$$

where T is the time needed to apply breaks [41]. Mitigating head-on collisions, where the velocity is essentially doubled, requires even greater warning distance.

For a forward-looking lidar system to cover a whole lane up to its apex, the half-horizontal viewing angle required is

$$\theta = \arccos \frac{R - W_{\text{L}}/2}{R}\,, \tag{13}$$

where W_{L} is lane width, and R is curve radius [41]. Hence, to enable scanning from 0.2m to 1.1m off the ground at the apex of a 125m curve, with a lane width 3.75m and a vehicle width 2m, the required FoV is $36.2° \times 10.2°$ [41].

The required angular resolution to detect cars, cyclists and pedestrians using modern open-source algorithms, such as PointPillars [42], is reported in Figure 7. This suggests that current technologies require an angular resolution $< 0.04°$ for safe operation at 200m. Furthermore, to enable object tracking, and to mitigate processing difficulties from the motion of the vehicle, a system must be able to capture at least 20 frames per second [22, 40, 41].

Combining these requirements, for 200m range, a direct time of flight detector must sample the environment around 5.8 million times per second. Assuming optimal operation with no down-time, the photon time of flight for this operation is around 8 seconds. Hence, multiple points must be scanned simultaneously to achieve the required performance. As discussed in §4, systems currently being brought to market claim to meet these requirements, but have yet to be independently tested.

3.2. Eye Safety

The most severe health risk associated with lidar operation is retinal heating. Hence, as has been previously reported [40, 41], lidar systems must comply with eye safety standards [43–45], which account for different combinations of wavelength, pulse duration, frame rate, number of pulses per frame and laser beam divergence. The IEC 60825-1 standard [45] requires the accessible emission limit (AEL) for operation to be the most restrictive of; "the maximum AEL for a single pulse (AEL.single), the average power for a pulse train of emission duration T (AEL.s.p.T) and the AEL for a single pulse multiplied by a correction factor determined by the effective number of pulses for a given exposure duration (AEL.s.p.train)" [41]. Representative AELs are given in Figure 8 for pulse lengths of 5ns using spot, blade, and flash illumination methods.

By assuming all emitted energy is collected by the retina and using Figure 8, the nominal ocular hazard distance (NOHD), beyond which the lidar pulses are safe, may be calculated. For a detection range of 200m, the NOHD for spot illumination is around 20m, considerably more than for blade or flash illuminations, with NOHDs of 0.03m and 0.17m, respectively [41]. These latter two distances could be covered within the body of a vehicle. The absorbance of light within the liquid part of the eye at wavelengths around 1550nm allows safe power levels 10-40 times greater than at 905nm, driving development at this wavelength [4].

3.3. Environmental Challenges

Autonomous driving will require lidar systems to perform well within rain, snow, fog, smoke and dust. This presents a significant challenge due to the absorbance and scattering of radiation by water (Figure 5). Many studies have investigated this effect. For example, [46, 47] compare using 905nm and 1550nm wavelengths in rain and fog, concluding that the significantly increased emission power possible at 1550nm can result in improved degraded-weather performance. Montalban [47] makes it clear that different rain droplet sizes have a significant effect on detection capability and suggests using multi-echo detection to quantify the environmental conditions; another method for this has also been proposed by Zhang [48].

Characterising the returns from adverse conditions enables the rejection of adverse reflections from airborne particles, particularly when recording the full lidar waveform [49, 50]. However, [51] reports that below 40m meteorological visibility, the perception limit for modern automotive lidar systems is less than 25m. Signal processing methods to mitigate these effects are an active research area, although some private companies claim to have solutions [57].

During real-world operation, lidar sensors will be subject to dirt accumulation - which has been shown to decrease sensor maximum range by up to 75% [52], along with significant interference from lidar systems in other vehicles. One solution to the latter of these challenges is to use FMCW lidar with identifying signatures encoded within the modulated signal [6].

4. Future Trends and Conclusions

Most self-driving systems use machine learning (ML) models to combine data from lidar and other sensors to achieve efficient, accurate detection of hazards and the surrounding environment [61–70]. Some systems also use this analysis to detect potential hazards to scan in more detail [71]. In the case of mobile hazards, cross-frame tracking can also help to improve detection

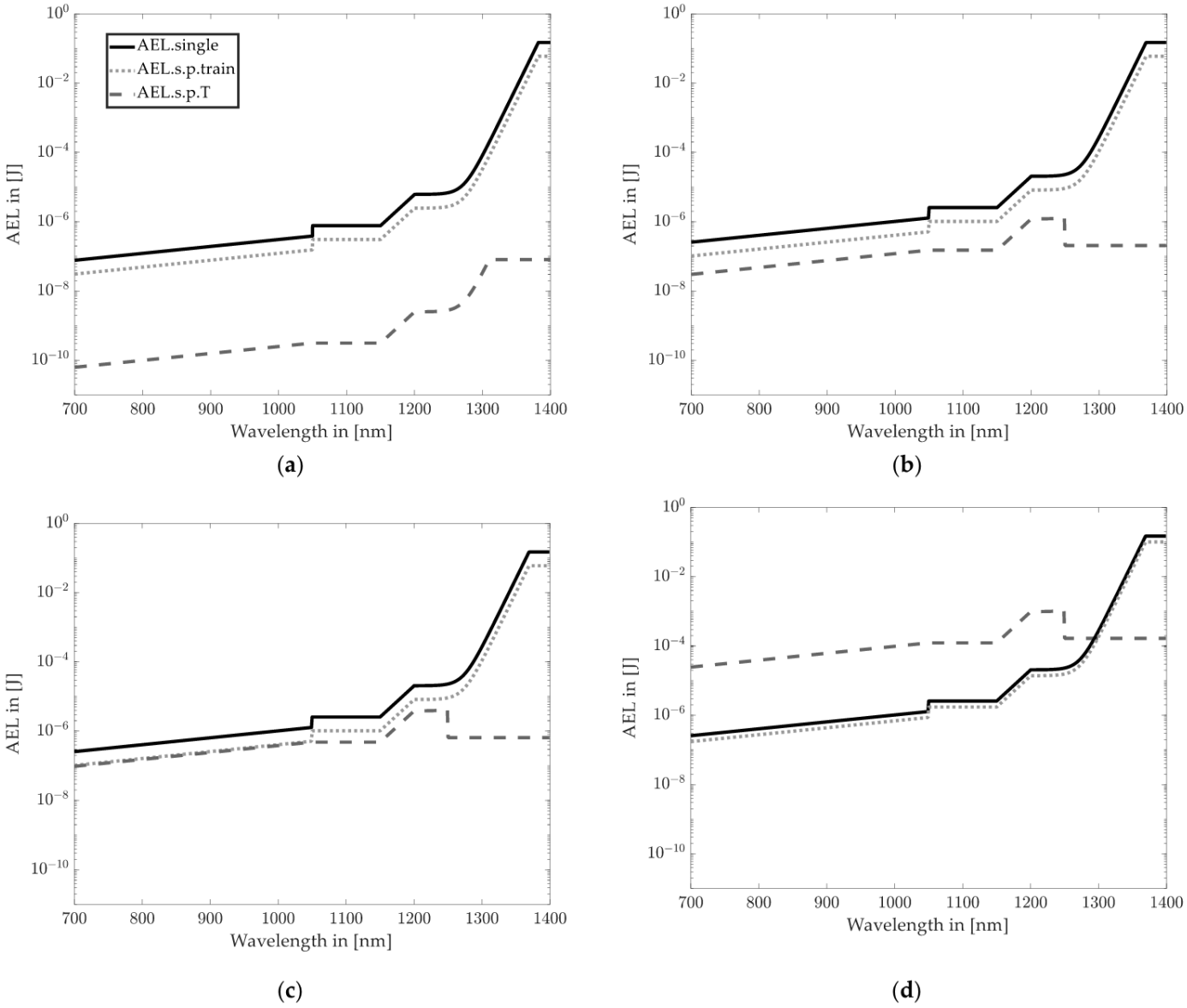

Fig. 8. Maximum AEL for (a) spot scanning, (b) horizontal blade illumination, (c) vertical blade illumination and (d) flash lidar systems [41].

reliability and predict the motion of the hazard [72, 73]. Unfortunately, there is a limited amount of publicly-available lidar training data, especially in adverse weather conditions, making model training difficult. Therefore, methods are being developed to computationally generate lidar datasets [74–76]. There are, however, concerns that using ML for self-driving applications could result in vulnerability to malicious attacks [77, 78].

Current developments in automotive lidar hardware focus mostly on solid-state lidar systems, either using MEMS or OPAs due to their superior durability. A summary of current and upcoming lidar products is given in Table 1. This highlights that many providers have produced eye-safe solutions which meet the angular resolution, range and FoV requirements described in §3.1 and §3.2. This is exciting, however, the costs of these systems are still not widely available and scientific testing of their performance is still required. Research is still ongoing to improve the coherency of laser technologies, SPAD quenching, lidar miniaturisation, system mass-production and system efficiency; continuing the trend of rapid advancement in automotive lidar technology.

Company	Mechanism	Range with $\beta = 0.1$ / m	Angular Resolution / °	Horizontal FoV / °	Vertical FoV / °	PPS / million	FPS	λ / nm	Availability
Cepton [53]	Solid-State	300	0.05	120	25	3.8	-	905	Now
Luminar [54]	Solid-State	300 for "Dark objects"	0.06	120	28	-	-	1550	Now
Aurora (Blackmore) [55]	FMCW, Solid State	400 expected	-	-	-	-	-	-	2027
Analog Photonics [56]	Solid-State OPA	-	-	-	-	-	-	-	2025
Ouster (Velodyne) [18]	Mechanical	300	0.2 Horizontal, 0.1 Vertical	360	40	-	20	905	Now
Ouster (Velodyne) [57]	Mechanical	200	-	360	22.5	2.62	20	-	Now
AEye [58]	Solid-State	325	0.025	120	30	6.2	-	1550	-
Innoviz [59]	Solid-State	300	0.05	120	43	-	10 or 20	905	Now
Hesai [60]	Solid-State	300	0.05	120	25.6	12.3	-	905	-

Table 1. A summary of current and upcoming automotive lidar technologies. PPS and FPS abbreviate pixels per second and frames per second respectively.

References

1. Velodyne Lidar *'History'* (no date). Available at: https://velodynelidar.com/history/ (Accessed: 21 April 2024).
2. Hecht, J. (no date) *Optics & Photonics News - Lidar for Self-Driving Cars*. Available at: http://www.optica-opn.org/home/articles/volume_29/january_2018/features/lidar_for_self-driving_cars/ (Accessed: 24 March 2024).
3. Li, Y. and Ibanez-Guzman, J. (2020) 'Lidar for Autonomous Driving: The Principles, Challenges, and Trends for Automotive Lidar and Perception Systems', *IEEE Signal Processing Magazine*, 37(4), pp. 50–61. Available at: https://doi.org/10.1109/MSP.2020.2973615.
4. Rablau, C.I. (2019) 'Lidar: a new self-driving vehicle for introducing optics to broader engineering and non-engineering audiences', in A.-S. Poulin-Girard and J.A. Shaw (eds) *Fifteenth Conference on Education and Training in Optics and Photonics: ETOP 2019. 15th Conference on Education and Training in Optics and Photonics, ETOP 2019*, Quebec City, Canada: SPIE, p. 138. Available at: https://doi.org/10.1117/12.2523863.
5. Zhao, F., Jiang, H. and Liu, Z. (2019) 'Recent development of automotive LiDAR technology, industry and trends', in *Eleventh International Conference on Digital Image Processing (ICDIP 2019). Eleventh International Conference on Digital Image Processing (ICDIP 2019)*, SPIE, pp. 1132–1139. Available at: https://doi.org/10.1117/12.2540277.
6. Royo, S. and Ballesta-Garcia, M. (2019) 'An Overview of Lidar Imaging Systems for Autonomous Vehicles', *Applied Sciences*, 9(19), p. 4093. Available at: https://doi.org/10.3390/app9194093.
7. Thakker, T. et al. (2019) 'LiDAR eyes for autonomous vehicles', in *AOS Australian Conference on Optical Fibre Technology (ACOFT) and Australian Conference on Optics, Lasers, and Spectroscopy (ACOLS) 2019. AOS Australian Conference on Optical Fibre Technology (ACOFT) and Australian Conference on Optics, Lasers, and Spectroscopy (ACOLS) 2019*, SPIE, pp. 85–86. Available at: https://doi.org/10.1117/12.2552778.
8. Tan, K. and Cheng, X. (2017) 'Specular Reflection Effects Elimination in Terrestrial Laser Scanning Intensity Data Using Phong Model', *Remote Sensing*, 9(8), p. 853. Available at: https://doi.org/10.3390/rs9080853.
9. Wandinger, U. (2005) 'Introduction to Lidar', in C. Weitkamp (ed.) *Lidar*. 1st edn. New York, NY, USA: Springer New York (Springer Series in Optical Sciences).
10. Wojtanowski, J. et al. (2014) 'Comparison of 905 nm and 1550 nm semiconductor laser rangefinders' performance deterioration due to adverse environmental conditions', *Opto-Electronics Review*, 22(3), pp. 183–190. Available at: https://doi.org/10.2478/s11772-014-0190-2.
11. Chen, J.-D. et al. (2022) '3-D Multi-Input Multi-Output (MIMO) Pulsed Chaos Lidar Based on Time-Division Multiplexing', *IEEE Journal of Selected Topics in Quantum Electronics*, 28(5: Lidars and Photonic Radars), pp. 1–9. Available at: https://doi.org/10.1109/JSTQE.2022.3150791.
12. Pierrottet, D. et al. (2008) 'Linear FMCW Laser Radar for Precision Range and Vector Velocity Measurements', *MRS Proceedings*, 1076, pp. 1076-K04-06. Available at: https://doi.org/10.1557/PROC-1076-K04-06.
13. NASA Spinoff (2020) *Doppler Lidar Makes Self-Driving Cars Safer*. Available at: https://spinoff.nasa.gov/Spinoff2020/t_8.html (Accessed: 15 March 2024).
14. Patole, S.M. et al. (2017) 'Automotive radars: A review of signal processing techniques', *IEEE Signal Processing Magazine*, 34(2), pp. 22–35. Available at: https://doi.org/10.1109/MSP.2016.2628914.
15. Doylend, J.K. and Gupta, S. (2020) 'An overview of silicon photonics for LIDAR', in *Silicon Photonics XV. Silicon Photonics XV*, SPIE, pp. 109–115. Available at: https://doi.org/10.1117/12.2544962.
16. Li, B., Lin, Q. and Li, M. (2023) 'Frequency–angular resolving LiDAR using chip-scale acousto-optic beam steering', *Nature*, 620(7973), pp. 316–322. Available at: https://doi.org/10.1038/s41586-023-06201-6.
17. Xu, Z. et al. (2017) 'Simultaneous Real-Time Ranging and Velocimetry via a Dual-Sideband Chirped Lidar', *IEEE Photonics Technology Letters*, 29(24), pp. 2254–2257. Available at: https://doi.org/10.1109/LPT.2017.2771415.
18. Ouster (no date) *VLS 128*. Available at: https://ouster.com/products/hardware/vls-128 (Accessed: 16 April 2024).
19. Hah, D. et al. (2004) 'Theory and Experiments of Angular Vertical Comb-Drive Actuators for Scanning Micromirrors', *IEEE Journal of Selected Topics in Quantum Electronics*, 10(3), pp. 505–513. Available at: https://doi.org/10.1109/JSTQE.2004.829200.
20. Holmstrom, S.T.S., Baran, U. and Urey, H. (2014) 'MEMS Laser Scanners: A Review', *Journal of Microelectromechanical Systems*, 23(2), pp. 259–275. Available at: https://doi.org/10.1109/JMEMS.2013.2295470.
21. Yoo, H.W. et al. (2018) 'MEMS-based lidar for autonomous driving', *e & i Elektrotechnik und Informationstechnik*, 135(6), pp. 408–415. Available at: https://doi.org/10.1007/s00502-018-0635-2.
22. Piatek, S. (no date) *LiDAR and Other Techniques*. Available at: https://www.hamamatsu.com/content/dam/hamamatsu-photonics/sites/static/hc/resources/W0004/lidar_webinar_12.6.17.pdf (Accessed: 16 April 2024).
23. Huang, Y. et al. (2012) 'MEMS Reliability Review', *IEEE Transactions on Device and Materials Reliability*, 12(2), pp. 482–493. Available at: https://doi.org/10.1109/TDMR.2012.2191291.
24. Lemmetti, J. et al. (2021) 'Long-range all-solid-state flash LiDAR sensor for autonomous driving', in *M.S. Zediker (ed.) High-Power Diode Laser Technology XIX. High-Power Diode Laser Technology XIX*, Online Only, United States: SPIE, p. 22. Available at: https://doi.org/10.1117/12.2578769.
25. Henley, C., Hollmann, J. and Raskar, R. (2022) 'Bounce-Flash Lidar', *IEEE Transactions on Computational Imaging*, 8, pp. 411–424. Available at: https://doi.org/10.1109/TCI.2022.3174802.
26. ThinkAutonomous (2023) *A Hardcore Look at 9 types of LiDAR systems*Available at: https://www.thinkautonomous.ai/blog/types-of-lidar/ (Accessed: 16 April 2024).
27. Hoffmann, G. (2007) 'Principles and working mechanisms of water-filtered infrared-A (wIRA) in relation to wound healing', *GMS Krankenhaushygiene interdisziplinar*, 2(2), p. Doc54.
28. Valley, S., L. (1965) 'Handbook of Geophysics and Space Environments'. Air Force Cambridge research labs Hanscom AFP MA. Available at: https://apps.dtic.mil/sti/citations/ADA056800.
29. Michalzik, R. (ed.) (2013) *VCSELs: Fundamentals, Technology and Applications of Vertical-Cavity Surface-Emitting Lasers*. Berlin, Heidelberg: Springer Berlin Heidelberg (Springer Series in Optical Sciences). Available at: https://doi.org/10.1007/978-3-642-24986-0.
30. Paschotta, R. (2019) 'VCSEL Arrays - an encyclopedia article', in *RP Photonics Encyclopedia*. RP Photonics AG. Available at: https://doi.org/10.61835/5in.
31. Seurin, J.-F. et al. (2008) 'High-power high-efficiency 2D VCSEL arrays', in C. Lei and J.K. Guenter (eds). *Integrated Optoelectronic Devices 2008*, San Jose, CA, p. 690808. Available at: https://doi.org/10.1117/12.774126.
32. Warren, M.E. et al. (2018) 'Low-divergence high-power VCSEL arrays for lidar application', in K.D. Choquette and C. Lei (eds) *Vertical-Cavity Surface-Emitting Lasers XXII*. Vertical-Cavity Surface-Emitting Lasers XXII, San Francisco, United States: SPIE, p. 14. Available at: https://doi.org/10.1117/12.2290937.
33. Seurin, J.-F. (2009) *Harnessing light for high-power applications*. Available at: https://spie.org/news/1638-harnessing-light-for-high-power-applications (Accessed: 18 April 2024).
34. Moser, A. and Latta, E.E. (1992) 'Arrhenius parameters for the rate process leading to catastrophic damage of AlGaAs-GaAs laser facets', *Journal of Applied Physics*, 71(10), pp. 4848–4853. Available at: https://doi.org/10.1063/1.350628.
35. Lauer, C. et al. (2023) 'Advances in 9xx nm edge-emitting high-power pulse laser diodes for LiDAR applications'.
36. Behringer, M. and Johnson, K. (2021) 'Laser lightsources for LIDAR', in *2021 27th International Semiconductor Laser Conference (ISLC). 2021 27th International Semiconductor Laser Conference (ISLC)*, Potsdam, Germany: IEEE, pp. 1–2. Available at: https://doi.org/10.1109/ISLC51662.2021.9615718.
37. McManamon, P.F. *et al.* (2017) 'Comparison of flash lidar detector options', *Optical Engineering*, 56(3), p. 031223. Available at: https://doi.org/10.1117/1.OE.56.3.031223.

38. Paschotta, R. (2008) 'Avalanche Photodiodes - an encyclopedia article', in *RP Photonics Encyclopedia*. RP Photonics AG. Available at: https://doi.org/10.61835/pbn.
39. Charbon, E. et al. (2013) 'SPAD-Based Sensors', in F. Remondino and D. Stoppa (eds) *TOF Range-Imaging Cameras*. Berlin, Heidelberg: Springer, pp. 11–38. Available at: https://doi.org/10.1007/978-3-642-27523-4_2.
40. Bastos, D. et al. (2021) 'An Overview of LiDAR Requirements and Techniques for Autonomous Driving', in *2021 Telecoms Conference (ConfTELE)*. 2021 Telecoms Conference (ConfTELE), pp. 1–6. Available at: https://doi.org/10.1109/ConfTELE50222.2021.9435580.
41. Dai, Z. et al. (2022) 'Requirements for Automotive LiDAR Systems', *Sensors*, 22(19), p. 7532. Available at: https://doi.org/10.3390/s22197532.
42. Lang, A.H. et al. (2019) 'PointPillars: Fast Encoders for Object Detection from Point Clouds'. arXiv. Available at: https://doi.org/10.48550/arXiv.1812.05784.
43. 'Safe use of Lasers, Z.136.1' (2022). American National Standards Institute.
44. 'Safe Use of Lasers Outdoors, Z136.6' (2015). American National Standards Institute.
45. 'Safety of Laser Products - Part 1: Equipment Classification and Requirements' (2014). International Electrotechnical Commission.
46. Kutila, M. et al. (2018) 'Automotive LiDAR performance verification in fog and rain', in *2018 21st International Conference on Intelligent Transportation Systems (ITSC). 2018 21st International Conference on Intelligent Transportation Systems (ITSC)*, Maui, HI: IEEE, pp. 1695–1701. Available at: https://doi.org/10.1109/ITSC.2018.8569624.
47. Montalban, K. et al. (2021) 'A Quantitative Analysis of Point Clouds from Automotive Lidars Exposed to Artificial Rain and Fog', in *Atmosphere*. Available at: https://www.mdpi.com/2073-4433/12/6/738 (Accessed: 24 March 2024).
48. Zhang, C. et al. (2021) 'LiDAR Degradation Quantification for Autonomous Driving in Rain', in *2021 IEEE/RSJ International Conference on Intelligent Robots and Systems (IROS). 2021 IEEE/RSJ International Conference on Intelligent Robots and Systems (IROS)*, pp. 3458–3464. Available at: https://doi.org/10.1109/IROS51168.2021.9636694.
49. Trickey, E., Church, P. and Cao, X. (2013) 'Characterization of the OPAL obscurant penetrating LiDAR in various degraded visual environments', in K.L. Bernier and J.J. Güell (eds). *PSPIE Defense, Security, and Sensing*, Baltimore, Maryland, USA, p. 87370E. Available at: https://doi.org/10.1117/12.2015259.
50. Wallace, A.M., Halimi, A. and Buller, G.S. (2020) 'Full Waveform LiDAR for Adverse Weather Conditions', *IEEE Transactions on Vehicular Technology*, 69(7), pp. 7064–7077. Available at: https://doi.org/10.1109/TVT.2020.2989148.
51. Bijelic, M., Gruber, T. and Ritter, W. (2018) 'A Benchmark for Lidar Sensors in Fog: Is Detection Breaking Down?', in *2018 IEEE Intelligent Vehicles Symposium (IV). 2018 IEEE Intelligent Vehicles Symposium (IV)*, pp. 760–767. Available at: https://doi.org/10.1109/IVS.2018.8500543.
52. Trierweiler, M. et al. (2019) 'Influence of sensor blockage on automotive LiDAR systems', in *2019 IEEE SENSORS. 2019 IEEE SENSORS*, Montreal, QC, Canada: IEEE, pp. 1–4. Available at: https://doi.org/10.1109/SENSORS43011.2019.8956792.
53. Cepton (no date) *Ultra*. Available at: https://www.cepton.com/products/ultra (Accessed: 21 April 2024).
54. Luminar (no date) *Technologies*. Available at: https://www.luminartech.com/technology#iris (Accessed: 21 April 2024).
55. Aurora (no date) *FirstLight Lidar—On a chip*. Available at: https://blog.aurora.tech/progress/firstlight-lidar-on-a-chip (Accessed: 21 April 2024).
56. IEEE Spectrum (2023) *Lidar on a Chip Puts Self-Driving Cars in the Fast Lane*. Available at: https://spectrum.ieee.org/lidar-on-a-chip (Accessed: 14 April 2024).
57. Ouster (no date) *Long-range lidar sensor for autonomous vehicles & trucking*. Available at: https://ouster.com/products/hardware/os2-lidar-sensor (Accessed: 21 April 2024).
58. AEye (no date) *AEye Announces In-Cabin Lidar That Maximizes Both Performance and Vehicle Design*. Available at: https://www.aeye.ai/press-releases/aeye-announces-in-cabin-lidar-that-maximizes-both-performance-and-vehicle-design/ (Accessed: 21 April 2024).
59. Innoviz (no date) *InnovizTwo*. Available at: https://innoviz.tech/innoviztwo (Accessed: 21 April 2024).
60. HESAI Technology (no date) *AT512 Automotive Ultra-High Resolution, Ultra-Long-Range Lidar*. Available at: https://www.hesaitech.com/product/at512/ (Accessed: 21 April 2024).
61. Zhang, Y. et al. (2022) 'An efficient LiDAR-based localization method for self-driving cars in dynamic environments', *Robotica*, 40(1), pp. 38–55. Available at: https://doi.org/10.1017/S0263574721000369.
62. Elhousni, M. and Huang, X. (2020) 'A Survey on 3D LiDAR Localization for Autonomous Vehicles'. arXiv. Available at: http://arxiv.org/abs/2006.00648 (Accessed: 24 March 2024).
63. Ouyang, Z. et al. (2017) 'A cGANs-Based Scene Reconstruction Model Using Lidar Point Cloud', in *2017 IEEE International Symposium on Parallel and Distributed Processing with Applications and 2017 IEEE International Conference on Ubiquitous Computing and Communications (ISPA/IUCC). 2017 IEEE International Symposium on Parallel and Distributed Processing with Applications and 2017 IEEE International Conference on Ubiquitous Computing and Communications (ISPA/IUCC)*, pp. 1107–1114. Available at: https://doi.org/10.1109/ISPA/IUCC.2017.00167.
64. Park, M., Kim, H. and Park, S. (2021) 'A Convolutional Neural Network-Based End-to-End Self-Driving Using LiDAR and Camera Fusion: Analysis Perspectives in a Real-World Environment', *Electronics*, 10(21), p. 2608. Available at: https://doi.org/10.3390/electronics10212608.
65. Zhou, S. et al. (2020) 'Deep SCNN-Based Real-Time Object Detection for Self-Driving Vehicles Using LiDAR Temporal Data', *IEEE Access*, 8, pp. 76903–76912. Available at: https://doi.org/10.1109/ACCESS.2020.2990416.
66. Gomes, T. et al. (2023) 'A Survey on Ground Segmentation Methods for Automotive LiDAR Sensors', *Sensors*, 23(2), p. 601. Available at: https://doi.org/10.3390/s23020601.
67. Zhang, Y. et al. (2018) 'Road-Segmentation-Based Curb Detection Method for Self-Driving via a 3D-LiDAR Sensor', *IEEE Transactions on Intelligent Transportation Systems*, 19(12), pp. 3981–3991. Available at: https://doi.org/10.1109/TITS.2018.2789462.
68. Chen, Shengjie et al. (2018) 'A Computationally Efficient Solution for LiDAR-Based Obstacle Detection in Autonomous Driving', in Y. Bi et al. (eds) *Embedded Systems Technology, ESTC 2017. 15th National Conference on Embedded Systems Technology (ESTC) - Embedded Systems and Intelligent Computing*, Berlin: Springer-Verlag Berlin (Communications in Computer and Information Science), pp. 43–62. Available at: https://doi.org/10.1007/978-981-13-1026-3_4.
69. Khan, D. et al. (2022) 'Multimodal Object Detection and Ranging Based on Camera and Lidar Sensor Fusion for Autonomous Driving', in *2022 27th Asia Pacific Conference on Communications (APCC). 2022 27th Asia Pacific Conference on Communications (APCC)*, pp. 342–343. Available at: https://doi.org/10.1109/APCC55198.2022.9943618.
70. Kumar, G.A. et al. (2020) 'LiDAR and Camera Fusion Approach for Object Distance Estimation in Self-Driving Vehicles', *Symmetry*, 12(2), p. 324. Available at: https://doi.org/10.3390/sym12020324.
71. Jovanov, L., Lee, W.-Y. and Philips, W. (2023) 'Adaptive point cloud acquisition and upsampling for automotive lidar', *Applied Optics*, 62(17), p. F8. Available at: https://doi.org/10.1364/AO.482535.
72. Tang, J. et al. (2020) 'Tracking to Improve Detection Quality in Lidar For Autonomous Driving', in *ICASSP 2020 - 2020 IEEE International Conference on Acoustics, Speech and Signal Processing (ICASSP). ICASSP 2020 - 2020 IEEE International Conference on Acoustics, Speech and Signal Processing (ICASSP)*, pp. 2683–2687. Available at: https://doi.org/10.1109/ICASSP40776.2020.9053041.
73. Sighencea, B.I., Stanciu, R.I. and Căleanu, C.D. (2021) 'A Review of Deep Learning-Based Methods for Pedestrian Trajectory Prediction', *Sensors*, 21(22), p. 7543. Available at: https://doi.org/10.3390/s21227543.
74. Lee, J. et al. (2022) 'GAN-Based LiDAR Translation between Sunny and Adverse Weather for Autonomous Driving and Driving Simulation', *Sensors*, 22(14), p. 5287. Available at: https://doi.org/10.3390/s22145287.
75. Manivasagam, S. et al. (2020) 'LiDARsim: Realistic LiDAR Simulation by Leveraging the Real World', in. *Proceedings of the IEEE/CVF Conference on Computer Vision and Pattern Recognition*, pp. 11167–11176. Available at: https://arxiv.org/abs/2006.09348 (Accessed: 7 February 2024).
76. Martinek, P. et al. (2020) 'Lidar-based Deep Neural Network for Reference Lane Generation', in *2020 IEEE Intelligent Vehicles Symposium (IV). 2020 IEEE Intelligent Vehicles Symposium (IV)*, pp. 89–94. Available at: https://doi.org/10.1109/IV47402.2020.9304623.
77. Zhang, Y. et al. (2022) 'Towards Backdoor Attacks against LiDAR Object Detection in Autonomous Driving', in *Proceedings of the 20th ACM Conference on Embedded Networked Sensor Systems. SenSys '22: The 20th ACM Conference on Embedded Networked Sensor Systems*, Boston Massachusetts: ACM, pp. 533–547. Available at: https://doi.org/10.1145/3560905.3568539.
78. Zhu, Y. et al. (2021) 'Can We Use Arbitrary Objects to Attack LiDAR Perception in Autonomous Driving?', in *Proceedings of the 2021 ACM SIGSAC Conference on Computer and Communications Security*. New York, NY, USA: Association for Computing Machinery (CCS '21), pp. 1945–1960. Available at: https://doi.org/10.1145/3460120.3485377.